Scientific Visualization, 2024, volume 16, number 1, pages 52 - 63, DOI: 10.26583/sv.16.1.05

Visualization of Flow of a Viscous Incompressible Fluid Corresponding to Exact Solutions of the Navier-Stokes Equations

V. A. Galkin[1,A,B], A.O. Dubovik[2,A,B], D.A. Morgun[3,A]

[A] Surgut Branch of SRISA
[B] Surgut State University

[1] ORCID: 0000-0002-9721-4026, val-gal@yandex.ru
[2] ORCID: 0000-0002-4158-9646, alldubovik@gmail.com
[3] ORCID: 0000-0003-0692-1583, morgun_da@office.niisi.tech

Abstract

The work visualizes flows corresponding to the exact solutions of the system of hydrodynamic equations previously published by the authors, consisting of the vector Navier-Stokes equation and the law of conservation of mass for an incompressible fluid. This work uses the MathGL library for the C/C++ language and ParaView for scientific visualization of the results of numerical and analytical calculations. Without the use of such means, it would be impossible to see that the fluid flow is stratified into invariant subregions, and the trajectories of motion of fluid particles are wound on torus-shaped surfaces.

Most of the scientific works on the study of hydrodynamic equations cover the results of calculations and do not address the questions of the existence of exact analytical solutions. At the same time, these calculations are performed with a specially selected set of fitting parameters unique to the equipment used and the computer software used. Questions about trust in the results of such calculations, their verification with exact solutions and the creation of a bank of test examples of applied problems in order to certify the applicability of the calculation results in practice become relevant.

Keywords: hydrodynamics, visualization of fluid flow, layered flow, exact solutions.

1. Introduction

Dynamics of a viscous incompressible fluid in the region D, $t>0$ determined by the vector velocity field $\mathbf{u}$ and pressure field p [1]:

$$\frac{\partial \mathbf{u}}{\partial t} + (\mathbf{u}\cdot\nabla)\mathbf{u} = -\frac{1}{\varrho_0}\nabla p + \mu\Delta\mathbf{u}, \tag{1}$$

$$\mathrm{div}\,\mathbf{u} = 0. \tag{2}$$

Here t is time, ϱ_0 is fluid density, μ is kinematic viscosity, $\varrho_0, \mu = const$. The pressure field p can be found from (1), (2) up to an additive term, which is an arbitrary function of time.

As boundary conditions, paragraphs 2 and 3 consider no-slip conditions

$$\mathbf{u}|_{\partial D} = 0. \tag{3}$$

In paragraphs 4 and 5, another boundary condition is valid no leakage

$$(\mathbf{u},\mathbf{n})|_{\partial D} = 0, \tag{4}$$

where the vector $\mathbf{n}$ is the normal to the boundary of the flow region ∂D. Boundary conditions in the tangent space to a manifold ∂D are given by narrowing the exact solutions.

This paper describes various classes of exact solutions of hydrodynamic equations satisfying (1) – (3) or (1), (2), (4), previously published in the authors' works [2–6]. Visualization of these classes of solutions allows, abstracting from the existing errors of computational fluid dynamics methods, to analyze the structure of highly entangled vortex flows. In

preparing this publication, the MathGL library (https://mathgl.sourceforge.net) and ParaView (https://www.paraview.org) were used.

For the oil and gas industry, the problem of mathematical modeling of fluid flow in a porous structure is relevant. Solving this problem opens the way to the creation of a domestic "digital field" technology [7], aimed at increasing the profitability of the hydrocarbon production process by controlling the dynamics of hydrocarbon-containing fluids in a porous medium, including due to thermal effects [8–11] and formation deformation [12].

The numerical solution of this class of problems involves the use of supercomputers and specially developed software. At the same time, calculations are performed with a specially selected set of fitting parameters [4], unique to the equipment used and the computer software used. In this regard, it is relevant to create a bank of test examples of precisely solvable non-stationary hydrodynamics problems in conditions of complex geometry, the use of which will allow one to verify the calculation results and evaluate their accuracy. Works [13–21] present the results of numerical modeling of three-dimensional fluid flows and estimates of their computational accuracy, and works [22–26] present some classes of exact solutions.

The region of fluid flow is a porous medium $D \equiv \mathrm{R}^n \backslash \partial D$, where ∂D is a discrete set of points that are nodes of a certain grid, and the adhesion condition (3) is satisfied. The grid consists of cells – squares (paragraph 2) or cubes (paragraph 3), the linear size of which is equal to 2π. By spatiotemporally replacing, one can obtain a grid whose cells have an arbitrary linear size. Further it is assumed $\varrho_0 = 1$.

2. Exact solutions in a plane periodic structure

Let us consider the exact solution [2, 3] of problem (1) – (3) in a flat domain D

$$\mathbf{u}|_{t=0} = \left\{\sin\left(\sqrt{\lambda}\,x_2\right);\sin\left(\sqrt{\lambda}\,x_1\right)\right\}, \qquad \lambda>0,$$

where $\left(x_1,x_2\right)$ denote Cartesian coordinates. Solution (5) takes place for the initial condition

$$\begin{aligned} \mathbf{u} &= e^{-\mu\lambda t}\left\{\sin\left(\sqrt{\lambda}\,x_2\right);\sin\left(\sqrt{\lambda}\,x_1\right)\right\}, \\ p &= e^{-2\mu\lambda t}\cos\left(\sqrt{\lambda}\,x_1\right)\cos\left(\sqrt{\lambda}\,x_2\right) \end{aligned} \tag{5}$$

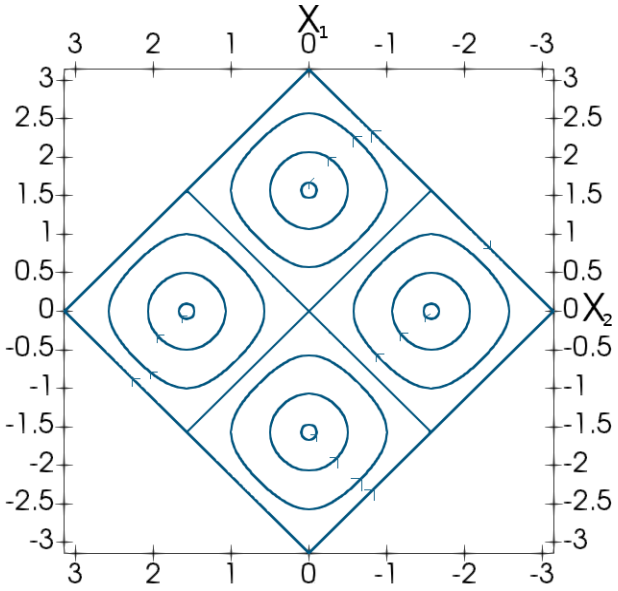

Fig. 1. Flow structure corresponding to solution (5) at $\lambda = 4$

The no-slip boundary condition (3) is satisfied at the points $\frac{\pi}{\sqrt{\lambda}} \times \mathbb{Z}_2$. Fig. 1 at $\lambda = 4$ illustrates the flow structure (5). In this case, the entire area is a union of squares with sides $\frac{\pi}{\sqrt{\lambda}}$, completely filling the flow area D. Inside these squares, the fluid moves along closed trajectories, with centers at the boundary points. These closed trajectories are diffeomorphic to two-dimensional torus, i.e., circles. The centers of the squares are located at the grid nodes ∂D. Along their boundaries, the liquid slides tangentially. The same effect was considered in [27] for the analytical solution of the equations of magnetic hydrodynamics, while the fluid slid along the boundary of the parallelepiped.

3. Exact solutions in a spatial periodic structure

Let us consider the exact solution [2–4] of problem (1) – (3) in the spatial domain D

$$\mathbf{u}|_{t=0} = \{\sin x_2 - \cos x_3; \sin x_3 - \cos x_1; \sin x_1 - \cos x_2\},$$

valid for the initial condition

$$\mathbf{u} = e^{-\mu t}\{\sin x_2 - \cos x_3; \sin x_3 - \cos x_1; \sin x_1 - \cos x_2\},\ p = -\frac{\mathbf{u}^2}{2}$$

and boundary condition (3).

In this case, the boundary of the flow region ∂D are the points $2\pi \times \mathbb{Z}_3 + \alpha_i$ and $2\pi \times \mathbb{Z}_3 + \pi(1,1,1) + \alpha_i$, where α_i one of the vectors of the set $0.25\pi \times \{(1,1,1),(1,-1,3),(3,1,-1),(-1,3,1)\}$.

Let us note the fact that time t affects only the vector length **u**, but not in his direction. When μ different from zero, the flow decays with time. The case $\mu = 0$ was considered by us earlier in [28]. When $\mu = 0$ for velocitiesu the continuity equation for an incompressible fluid is satisfied $\nabla \cdot \mathrm{u} = 0$, and the field u satisfies the stationary Euler equation

$(\mathrm{u} \cdot \nabla \mathrm{u}) = -\nabla \Phi$,

where $\Phi(x_1, x_2, x_3) = -\frac{3}{2} + (\sin x_1 \cos x_2 + \sin x_2 \cos x_3 + \sin x_3 \cos x_1)$.

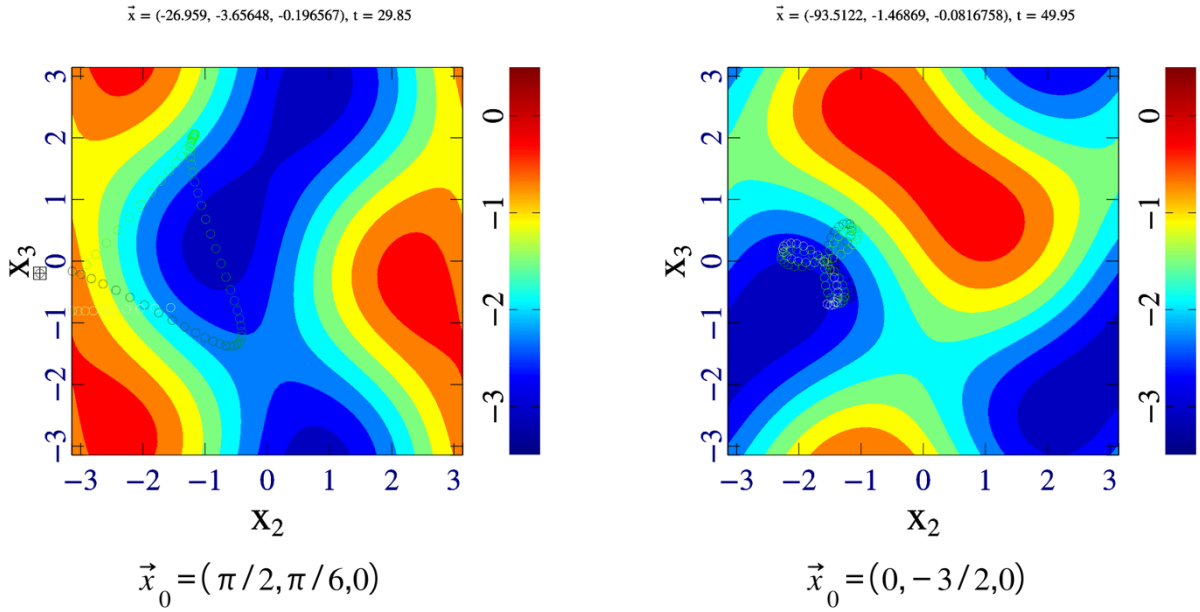

$\vec{x}_0 = (\pi/2, \pi/6, 0)$ $\vec{x}_0 = (0, -3/2, 0)$

Fig. 2. Particle trajectory against the background of potential level lines Φ, constructed in a plane, orthogonal Ox_1 to the current valuex_1 for two trajectories with different$\vec{x}_0$

In [28], we presented the following method, convenient for visual analysis of such problems. Let the trajectory plunge into the computational domain over time along a certain coordinate (x_1, x_2 or x_3). Let's select the appropriate coordinate axis and, in a plane orthogonal to it, we will construct potential level lines Φ for the current value of the "immersion coordinate." On the graph of level lines, we denote the current calculated point with a square, and a number of previous trajectory points we denote with circles. Let's take such graphs for the current calculated point and several previous ones and form an animation from them, which can be used to visually track the dynamics of the trajectory against the background of the potential, see Fig. 2.

The trajectory of a particle in such an animation demonstrates a certain smoothly rotating figure that plunges into the computational domain following the current point of the trajectory. Depending on the starting point of the trajectory, the figure formed by the trajectory also changes; in some cases the figure resembles an acute triangle, in others it resembles a rounded petal, in others it takes on intermediate forms.

4. Exact solutions in a ball and spherical layers

Let denote by ϱ_k non-negative roots of the equation

$$\operatorname{tg} R = R, \qquad R \geq 0,$$

sorted by ascending numbers $k \in \mathbb{N}$:

$$0 = \varrho_0 < \varrho_1 < \ldots < \varrho_k < \ldots$$

In this case, there is an asymptotic estimate at $k \to \infty$

$$\varrho_k \sim \frac{\pi}{2} + k\pi.$$

Considering a three-dimensional region $D \subset \mathbb{R}_3 = \left\{\mathbf{x} = \left(x_1, x_2, x_3\right)\right\}$. Let denote B_{ϱ_k} is the ϱ_k radius ball, i.e.

$$B_{\varrho_k} = \left\{\mathbf{x} \in \mathbb{R}_3 : \|x\| \overset{def}{=} \left(\sum_{i=1}^{3} x_i^2\right)^{\frac{1}{2}} < \varrho_k\right\}, \qquad k = 1,2,\ldots,$$

and B_{ϱ_k,ϱ_l} is the spherical layer with radiuses ϱ_k and ϱ_l, i. e.

$$B_{\varrho_k,\varrho_l} = \left\{\mathbf{x} \in \mathbb{R}_3 : \ \varrho_k < \|\mathbf{x}\| < \varrho_l\right\}.$$

The ball boundary B_{ϱ_k} let's denote $S_{\varrho_k} \overset{def}{=} \partial B_{\varrho_k}$, i. e. S_{ϱ_k} is radius boundary ϱ_k. For each vector $\mathbf{x} \in \mathbb{R}_3$ denoted by the symbol $r = \|x\|$ its Euclidean norm.

Let put

$$\bar{u}(r) = \begin{cases} r^{-1}\sin(r), & r > 0, \\ 1, & r = 0. \end{cases}$$

Let $\mathbf{x} \in \mathbb{R}_3 \backslash \{0\}$, $\alpha = (\alpha_1, \alpha_2, \alpha_3) \in \mathbb{R}_3$. Consider the vector field

$$\mathbf{U}_\alpha(\mathbf{x}) = \left\{ \frac{\bar{u}'(r)}{r} \begin{bmatrix} x_2 & -2 & -x_3 \\ -x_1 & x_3 & -2 \\ -2 & -x_2 & x_1 \end{bmatrix} + \frac{1}{r^2}\left(\bar{u}''(r) - \frac{\bar{u}'(r)}{r}\right) \begin{bmatrix} x_1x_3 & -\left(x_2^2+x_3^2\right) & x_1x_2 \\ x_2x_3 & x_1x_2 & -\left(x_1^2+x_3^2\right) \\ -\left(x_1^2+x_2^2\right) & x_1x_3 & x_2x_3 \end{bmatrix} \right\} \begin{pmatrix} \alpha_1 \\ \alpha_2 \\ \alpha_3 \end{pmatrix}.$$

In [5] it is shown that $\mathbf{U}_\alpha(\mathbf{x})$ you can continue in the class of infinitely differentiable functions C^∞ for the entire space $\mathbb{R}_3$ and the theorem is proven:

Theorem. Let the vector field

$$\mathbf{u}_{\alpha}(\mathbf{x},t) = \mathbf{U}_{\alpha}(\mathbf{x})\exp(-\mu t), \quad \mathbf{x} \in \mathbb{R}_3, \quad t \geq 0 \tag{6}$$

and scalar function

$$p(x,t) = -\frac{\varrho_0}{2}\left(\mathbf{u}_{\alpha}(\mathbf{x},t),\mathbf{u}_{\alpha}(\mathbf{x},t)\right) + \beta(t), \tag{7}$$

where $\beta(t)$ *is an arbitrary time-dependent function. Then a couple* $\{u_{\alpha},p\}$ *is a solution to the system of Navier–Stokes equations* (1), (2) *in the region* $D = \{\mathbf{x} \in \mathbb{R}_3\}$. *Moreover, on the boundary* S_{ϱ_k} *of each ball* B_{ϱ_k}, $k = 1,2,\ldots$ *the sliding conditions* (4) *are satisfied, i.e. formulas* (6), (7) *give a solution to problem* (1), (2), (4) *in each spatial ball* $D = B_{\varrho_k}$ *and spherical layer* $D = B_{\varrho_k,\varrho_l}$, $1 \leq k < l \leq +\infty$. (*Equality* $l = +\infty$ *by definition means that* $D = \mathbb{R}_3 \setminus (B_{\varrho_k} \cup S_{\varrho_k})$). *Vector velocity field* (6), *considered in the region* $D = \{\mathbf{x} \in \mathbb{R}_3\}$ *and spherical layers* $D = \mathbb{R}_3 \setminus (B_{\varrho_k} \cup S_{\varrho_k})$, *tends to zero as* $\|\mathbf{x}\| \to \infty$.

Let's limit ourselves to the case $\alpha = (\alpha_1,\alpha_2,\alpha_3) = (1,0,0)$, then the expression for $\mathbf{U}_{\alpha}(\mathbf{x})$ will be simplified and take the form

$$\mathrm{V} = \begin{pmatrix} \bar{u}'(r)\frac{x_2}{r} + \bar{u}''\frac{x_1x_3}{r^2} - \bar{u}'(r)\frac{x_1x_3}{r^3} \\ -\bar{u}'(r)\frac{x_1}{r} + \bar{u}''\frac{x_2x_3}{r^2} - \bar{u}'(r)\frac{x_2x_3}{r^3} \\ -\bar{u}'(r)\frac{2}{r} + \bar{u}'\frac{x_1^2+x_2^2}{r^3} - \bar{u}''(r)\frac{x_1^2+x_2^2}{r^2} \end{pmatrix}$$

Table 1 Roots of the equation $\mathrm{tg}(r) = r$ is no-flow boundaries

ϱ_0	0.00000000000000
ϱ_1	4.49340945790906
ϱ_2	7.72525183693771
ϱ_3	10.9041216594289
ϱ_4	4.49340945790906

In accordance with the theorem, the conditions of non-flow are satisfied

$$(\mathbf{V}(x,t),\mathbf{n}(x))\big|_{x \in \partial D} = 0$$

at the boundaries of spheres with radiuses $r = \varrho_k$, where ϱ_k is non-negative roots of the equation $\mathrm{tg}(r) = r$, sorted by ascending numbers. Multiple values ϱ_k are given in the table 1.

Visualization of the numerical simulation results demonstrates “stratification” along the spherical layers. Figure 3 shows trajectory animations for the first and second spherical layers. It can be seen that the trajectory of the point, which is determined by the vector field (4) and numerically simulated by solving the Cauchy problem for the corresponding equation of motion, actually remains within the selected spherical layer. Note that movement along the vertical axis in adjacent spherical layers occurs in opposite directions.

From the animation presented in Figure 4, one can get an idea of all possible trajectories that can be realized in the inner ball (Figure 4, left) or in the spherical layers (Figure 4, right).

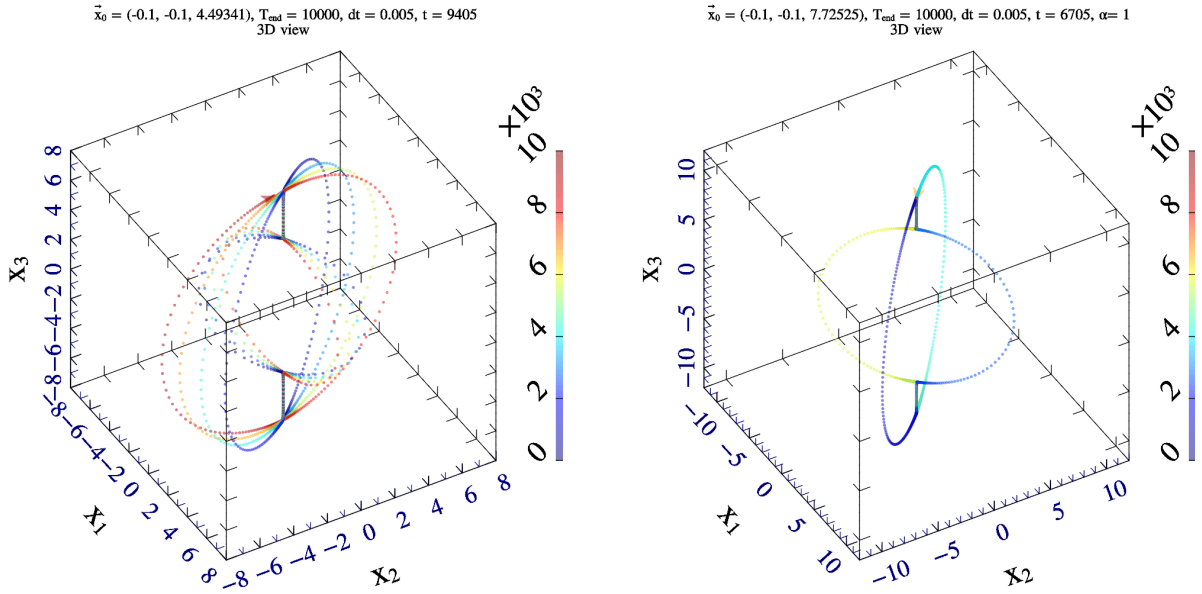

Fig. 3. Visualization of the trajectory. Left: starting point $\vec{x}_0 = (-0.1, -0.1, 4.49341)$ defined inside the first spherical layer $\varrho_1 < r < \varrho_2$, near the sphere $r = \varrho_1$. Right: starting point $\vec{x}_0 = (-0.1, -0.1, 7.72525)$ defined inside the second spherical layer $\varrho_2 < r < \varrho_3$, near the sphere $r = \varrho_2$.

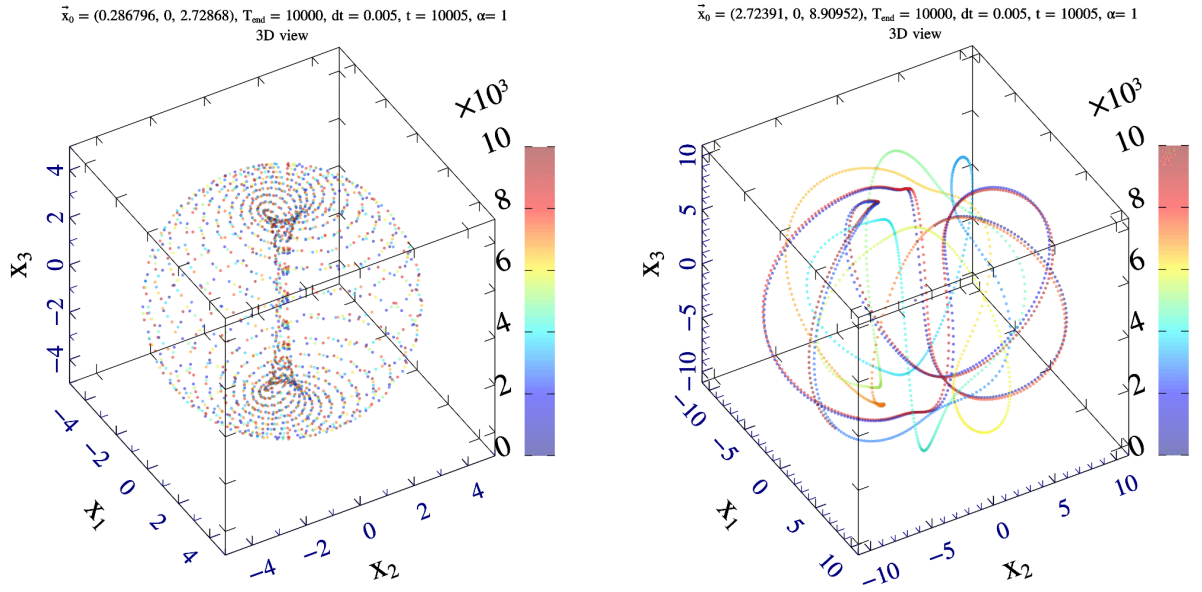

Fig. 4. Visualization of the dependence of trajectories on the starting point $\vec{x}_0 = (r, \varphi, \theta)$. The point changes with the value $\theta = 1°$ (position near the vertical axis) to the value $\theta = 90°$ (position near the equator). On the left is an animation for the inner ball. $r < \varrho_1$; on the right – animation for the second spherical layer $\varrho_2 < r < \varrho_3$.

5. Exact solutions in a cylinder and cylindrical layers

Let D is the three-dimensional flow area, $D \subset \mathbb{R}_3 = \left\{\mathbf{x} = \left(x_1, x_2, x_3\right)\right\}$. We will consider the system of equations (1), (2), (4) in cylinder C_k and coaxial cylinder C_{k_1,k_2}

$$C_k = \left\{\mathbf{x} \in \mathbb{R}^3 : 0 < r(\mathbf{x}) < \varrho_k, 0 < x_3 < 2\pi\sqrt{2}\right\},\ k \in \mathbb{N},$$

$$C_{k_1,k_2} = \left\{\mathbf{x} \in \mathbb{R}^3 : \varrho_{k_1} < r(\mathbf{x}) < \varrho_{k_2}, 0 < x_3 < 2\pi\sqrt{2}\right\}, \qquad k_1, k_2 \in \mathbb{N}, \qquad k_1 \neq k_2,$$

where $r(\mathbf{x}) = \sqrt{x_1^2 + x_2^2}$, $\varrho_k > 0$ are roots of the equation ordered in ascending order

$$J'_0\left(\frac{\varrho_k}{\sqrt{2}}\right) = 0, \qquad k \in \mathbb{N},$$

where $J_0(r)$ are Bessel function of the first kind of zero order.

Consider the vector field $\mathbf{U}(\mathbf{x})$, defined in the area $\mathbb{R}^3 \setminus \{r = 0\}$

$$\mathbf{U}(\mathbf{x}) = \frac{J'_0\left(\frac{r}{\sqrt{2}}\right)}{r\sqrt{2}} \begin{bmatrix} x_2 \sin\left(\frac{x_3}{\sqrt{2}}\right) + \frac{x_1}{\sqrt{2}} \cos\left(\frac{x_3}{\sqrt{2}}\right) \\ -x_1 \sin\left(\frac{x_3}{\sqrt{2}}\right) + \frac{x_2}{\sqrt{2}} \cos\left(\frac{x_3}{\sqrt{2}}\right) \\ 0 \end{bmatrix} + \frac{1}{2} J_0\left(\frac{r}{\sqrt{2}}\right) \begin{bmatrix} 0 \\ 0 \\ \sin\left(\frac{x_3}{\sqrt{2}}\right) \end{bmatrix}. \tag{8}$$

In [6] it is shown that the function $\mathbf{U}(\mathbf{x})$ has a continuation in the class of infinitely differentiable functions $C^\infty(\mathbb{R}^3)$ throughout space $\mathbb{R}^3$ and the theorem is true:

Theorem. *Let the vector field a* $\mathbf{u}(\mathbf{x},t)$ *and scalar field* $p(\mathbf{x},t)$ *look like*

$$\mathbf{u}(\mathbf{x},t) = \mathbf{U}(\mathbf{x}) e^{-\mu t},\ \mathbf{x} \in \mathbb{R}^3, t \geq 0, \tag{9}$$

$$p(\mathbf{x},t) = -\frac{\varrho_0}{2} \mathbf{u}^2(\mathbf{x},t) + \alpha(t), \tag{10}$$

where $\alpha(t)$*is an arbitrary function of time t. Then a couple* $\{\mathbf{u}(\mathbf{x},t), p(\mathbf{x},t)\}$ *is a solution to the system of Navier–Stokes equations* (1), (2) *in the region* $D = \{\mathbf{x} = \mathbb{R}^3\}$. *At the boundary of the region of each cylinder* $C_k = \left\{\mathbf{x} \in \mathbb{R}^3 : 0 < r(\mathbf{x}) < \varrho_k, 0 < x_3 < 2\pi\sqrt{2}\right\}$, $k \in \mathbb{N}$ *the sliding condition* (4) *is satisfied, i.e. expressions* (9), (10) *give solutions to problem* (1), (2), (4) *in each cylinder* $D = C_k$ *and cylindrical layer* $D = \amalg_{k,l}$, $k, l \in \mathbb{N}$, $k \neq l$. *Vector field* (8), *considered in* $D = \{\mathbf{x} = \mathbb{R}^3\}$ *and cylindrical layers* $D = \mathbb{R}^3 \setminus \left(\overline{C}_k\right)$ *tends to zero as* $r \to \infty$.

The fluid flow corresponding to solution (9), (10) is also divided into invariant subregions. These are the top and bottom halves of the cylinder. In Fig. 5–7 illustrate the evolution of the flow of one point of fluid, considered in the upper half of the cylinder, under the action of vector field (8). The resulting trajectories, described over time, are diffeomorphic to torus. For a point taken from the lower half of the cylinder, the flow structure is similar. It is only necessary to take into account the symmetry relative to the plane $x_3 = \pi\sqrt{2}$ In Fig. 5 shows the trajectory of the point $\left(\varrho_1 - \varepsilon, \varrho_1 - \varepsilon, 2\pi\sqrt{2} - \varepsilon\right)$, taken near the surface of the cylinder at $\varepsilon = 10^{-4}$, over time, in Fig. 6 illustrates the configuration of its path at a later point in time.

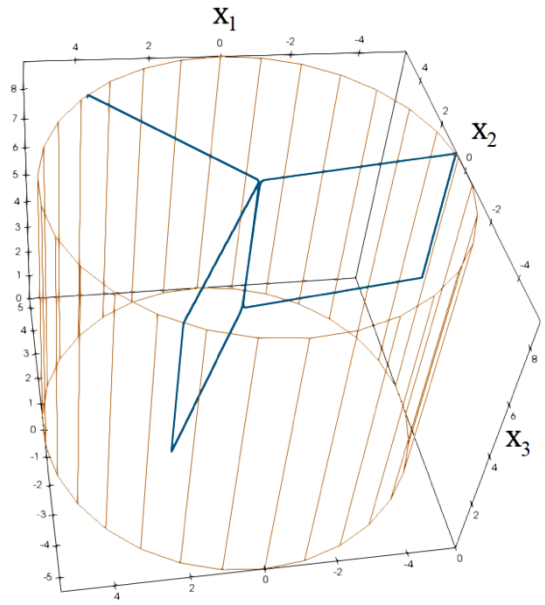

Fig. 5. Evolution of the flow of a fluid point $\left(\varrho_1-\varepsilon,\varrho_1-\varepsilon,2\pi\sqrt{2}-\varepsilon\right)$, appropriate (8)

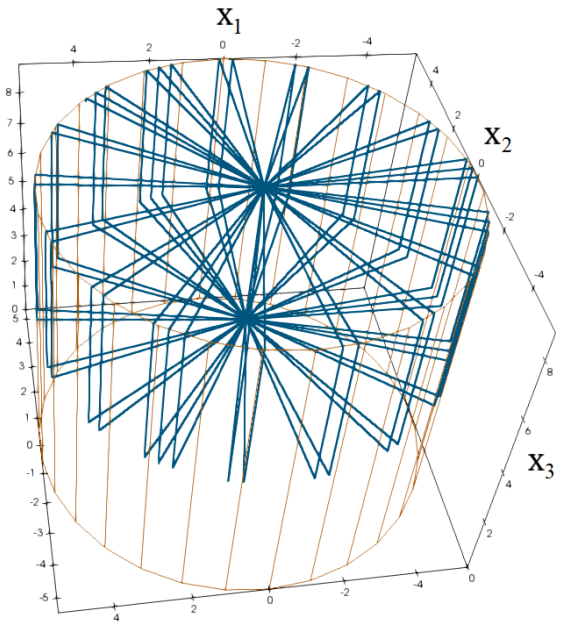

Fig. 6. Evolution of the flow of a fluid point $\left(\varrho_1-\varepsilon,\varrho_1-\varepsilon,2\pi\sqrt{2}-0.1\right)$, appropriate (8), over time

In Fig. 7 shows the trajectory of the point $\left(\varrho_1-\varepsilon,\varrho_1-\varepsilon,2\pi\sqrt{2}-\varepsilon\right)$, taken inside the top half of the cylinder, over time.

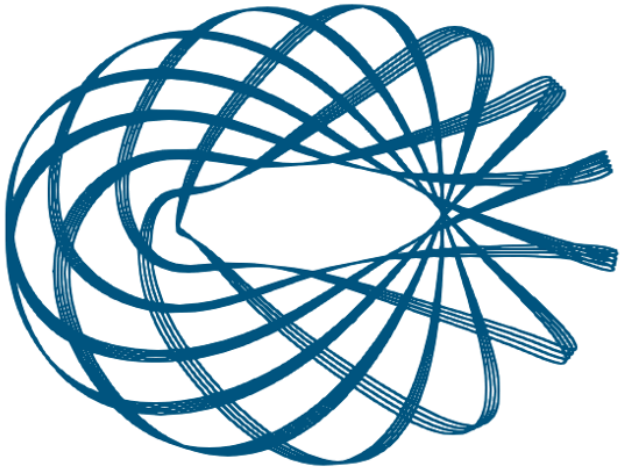

Fig. 7. Evolution of the flow of a fluid point $\left(\varrho_1 - \varepsilon, \varrho_1 - \varepsilon, 2\pi\sqrt{2} - 0.1\right)$, appropriate (8), over time

6. Conclusion

The article is devoted to the issues of visualization of numerical and analytical calculations of solutions to hydrodynamic equations describing the flow of a viscous incompressible fluid. The use of scientific visualization tools such as the MathGL library (https://mathgl.sourceforge.net) and ParaView (https://www.paraview.org) allows you to examine the structure of complex three-dimensional flows in more detail and analyze the results of their modeling.

The work was carried out within the framework of the state assignment of the Federal State Institution "Scientific Research Institute for System Analysis of the Russian Academy of Sciences (Performing fundamental scientific research GP 47) on topic No. 0580-2021-0007 “Development of methods for mathematical modeling of distributed systems and corresponding calculation methods.”

References

1. Landau L.D. Lifshits E. M. Teoreticheskaya fizika: Uchebn. posob.: Dlya vuzov. V 10 t. T. VI. Hydrodynamica [Theoretical physics: Textbook. manual: For universities. In 10 volumes, V. VI. Continuous media electrodynamics.] –Moscow: FIZMATLIT. 2001. 736 p. [in Russian]

2. Betelin V.B., Galkin V.A., Dubovik A.O. Exact Solutions of Incompressible Navier–Stokes Equations in the Case of Oil and Gas Industrial Problems // Doklady Mathematics. 2020. V. 102. No 3. p. 456–459.

3. Galkin V.A., Dubovik A.O. Visualization of flows of a viscous conductive liquid with the presence of impurities in the flow field corresponding to exact solutions of the MHD equations // Scientific Visualization. 2021. V. 13. No. 1. p. 104–123.

4. Betelin V.B., Galkin V.A. Mathematical and computational problems associated with the formation of structures in complex systems // Computer Research and Modeling. 2022, V. 14, No. 4. p. 805-815. [in Russian]

5. Galkin V.A. On a Class of Exact Solutions to the Incompressible Navier–Stokes System in a Ball and a Spherical Layer // Computational Mathematics and Mathematical Physics. 2023. V. 63. I. 6. p. 1064–1069.

6. Galkin V.A., Dubovik A.O. On one class of exact solutions of the system of Navier-Stokes equations for an incompressible fluid // Zhur. Math. model. 2023. V. 35. No. 8. p. 3–13. [in Russian]

7. Betelin V.B., Galkin V.A. Control of Incompressible Fluid Parameters in the case of Time_Varying Flow Geometry // Doklady Mathematics. 2015. V. 92. No. 1. p. 511–513.
8. Galich N.E. Teplovaya neustoychivost' i proboy dvizhushchikhsya vyazkikh zhidkostey v elektricheskom pole i pri pogloshchenii sveta [Thermal instability and breakdown of moving viscous fluids in electric field and absorption of light] // Zhurnal tekhnicheskoy fiziki. 1989. vol. 59. no. 7. p. 10–17. [in Russian]
9. Altoiz B.A., Savin, N.V., Shatagina, E.A. Effect of heat release in a microinterlayer of a liquid on the measurement of its viscosity // Tech. Phys. 2014.V. 59. I. 5. p. 649-655.
10. Kushtanova G.G. Fizika geosfery [Physics of the geosphere]. Kazan. From Kazan State University. 2004. 44 p. [in Russian]
11. Semenov N.N. Tsepnyye reaktsii [Chain reactions]. Moscow: Gomkhimtekhizdat. 1934. [in Russian]
12. Shestakov V.M. Hydrogeodynamica [Hydrogeodynamics]. Moscow: Moscow State University. 1995. 368 p. [in Russian]
13. Ahmed H. F., Malik F. K., Khan M. M. Influence of passive wake control on thermal-hydraulic performance of a cylinder confined in wavy channel under high blockage ratios // Thermophysics and Aeromechanics. 2022. V. 29. I. 3. p. 371–388.
14. Delnov V.N. Application of flow patterns and accounting of hydrodynamic effects in the course of upgrading distribution header systems of npp heat exchangers and reactors // Problems of Atomic Science and Technology. Series: Nuclear and Reactor Constants. 2021. I. 2. 2:14. [in Russian].
15. Renev M. E., Safronova Yu. F., Stishkov Yu. K. Controlling the Flow around a Circular Cylinder by Means of a Corona Discharge // Technical Physics. 2019. V. 64. I. 9. p. 1275–1282.
16. Khoroshev A.S., Shakhov V.G. The Intensity of Convection of Fluids With Different Prandtl Number in a Vertical Cylinder of Large Aspect Ratio // Mathematical Physics and Computer Simulation. 2018. V. 21 No. 1. p. 70–79. [in Russian].
17. Antuono M., Sun P. N., Marrone S., Colagrossi A. The δ–ALE–SPH model: an arbitrary Lagrangian-Eulerian framework for the δ–SPH model with Particle Shifting Technique. Computer & Fluids. 2020;104806.
18. Mohammed A. and others. CFD and statistical approach to optimize the average air velocity and air volume fraction in an inert-particles spouted-bed reactor (IPSBR) system. Heliyon. 2021;7(3):E06369.
19. Ren X., Xu K., Shyy W. A multi-dimensional high-order DG-ALE method based on gas-kinetic theory with application to oscillating bodies. Journal of Computational Physics. 2016;316:700–720.
20. Elgeti S., Sauerland H. Deforming fluid domains within the finite element method: five mesh based tracking methods in comparison. Archives of Computational methods in Engineering. 2016;23:323–361.
21. Burago N. G., Nikitin I. S., Yakushev V. L., “Application of overlapping meshes to flow computation in domains of variable geometry,” Proceedings of the 20th International Conference on Computational Mechanics and Modern Applied Systems (2017), p. 395–397. 2017:395–397.
22. Knyazev D. V., Kolpakov I. Y. The exact solutions of the problem of a viscous fluid flow in a cylindrical domain with varying radius // Russian Journal of Nonlinear Dynamics. 2015;11(1):89–97. [in Russian].
23. Trkal V. A note on the hydrodynamics of viscous fluids // Czechoslovak Journal of Physics. 1994. V. 44. No. 2. p. 97–106.
24. Sheretov Yu. V., “On solutions of the Cauchy problem for a quasi-hydrodynamic system,” Vestn. Tver. Gos. Univ. Ser. Prikl. Mat. 2020. No. 1. p. 84–96. [in Russian].
25. Arnol’d V. "Sur la topologie des ecoulements stationnaires des fluides parfaits". C. R. Acad. Sci. Paris, 261:17–20, 1965.

26. Bogoyavlenskij O. I., “On the Kelvin’s 1880 problem and exact solutions of the Navier–Stokes equations,” Steklov Mathematical Institute Seminar “Mathematics and Its Applications,” May 21, 2015, Moscow, Conference Hall(Gubkina 8). [in Russian].

27. Betelin V.B., Galkin V.A., Gorelikov A.V. Predictor–Corrector Algorithm for the Numerical Solution of the Magnetic Field Equation in Viscous Incompressible MHD Problems // Doklady Mathematics. 2015. V. 92. No. 2. p. 618–621.

28. Galkin V. A., Morgun D. A. Modeling and Visualization of Particle Trajectories Driven by an Asymmetric Potential // Russian Jourbal of Cybernetics. 2022. V.3. No 3. p. 8–13. [in Russian].